Neuron
Article

Rhythmic Modulation of Theta Oscillations Supports Encoding of Spatial and Behavioral Information in the Rat Hippocampus

Colin Molter,[1,2,3,4,*] Joseph O'Neill,[1,2] Yoko Yamaguchi,[3] Hajime Hirase,[5,6] and Xavier Leinekugel[1,2,5,*]
[1]Université de Bordeaux, Institut des Maladies Neurodégénératives, UMR 5293, F-33000 Bordeaux, France
[2]CNRS, Institut des Maladies Neurodégénératives, UMR 5293, F-33000 Bordeaux, France
[3]Dynamics of Emergent Intelligence, Riken Brain Science Institute (BSI),Wako-shi, Saitama, 351-0198, Japan
[4]Laboratory of Computational Neuroscience, EPFL, CH-1015 Lausanne, Switzerland
[5]Center of Molecular Biology and Neuroscience, Buzsaki-Lab, Newark, NJ 07102, USA
[6]Hirase Research Unit, Riken BSI, Wako-shi, Saitama, 351-0198, Japan
*Correspondence: colin.molter@gmail.com (C.M.), xlkg1@free.fr (X.L.)
http://dx.doi.org/10.1016/j.neuron.2012.06.036

SUMMARY

Oscillatory patterns of activity in various frequency ranges are ubiquitously expressed in cortical circuits. While recent studies in humans emphasized rhythmic modulations of neuronal oscillations ("second-order" rhythms), their potential involvement in information coding remains an open question. Here, we show that a rhythmic (~0.7 Hz) modulation of hippocampal theta power, unraveled by second-order spectral analysis, supports encoding of spatial and behavioral information. The phase preference of neuronal discharge within this slow rhythm significantly increases the amount of information carried by action potentials in various motor/cognitive behaviors by (1) distinguishing between the spikes fired within versus outside the place field of hippocampal place cells, (2) disambiguating place firing of neurons having multiple place fields, and (3) predicting between alternative future spatial trajectories. This finding demonstrates the relevance of second-order spectral components of brain rhythms for decoding neuronal information.

INTRODUCTION

Distinct behaviors are associated with distinct patterns of activity, presumably underlying specific cognitive functions. In the hippocampus, immobility, slow-wave sleep, and automatic behaviors (sniffing, chewing, champing, grooming, etc.) are accompanied by intermittent sharp-wave ripples (SPW) at high frequency (150–200 Hz), while locomotion, attention and REM sleep are accompanied by continuous theta oscillation (5–10 Hz) (Vanderwolf, 1969; Whishaw, 1972). These oscillations have been hypothesized to provide a common temporal reference for distributed neurons and support temporal coding, as illustrated in place cells' theta phase precession where the phase of a cell's spikes, relative to theta oscillations, systematically varies with the animal's position within its place field, so that additional spatial information is specifically carried by the phase of spike discharge within the theta cycle (Huxter et al., 2003, 2008; O'Keefe and Recce, 1993; Skaggs et al., 1996). Therefore, depending on brain state, neuronal populations oscillate at various frequencies which regulate the timing of neuronal interactions to support neuronal encoding and information processing. A related phenomenon, although less well understood, lies in the cyclic modulation of LFP oscillations or cross-frequency coupling (Bragin et al., 1995; Chrobak and Buzsáki, 1998). Recent studies in humans and monkeys emphasized the expression of rhythmic modulations of neuronal oscillations (Canolty et al., 2006; Drew et al., 2008; Lakatos et al., 2005; Lakatos et al., 2008; Leopold et al., 2003; Nir et al., 2008), but the potential involvement of these "second-order" rhythms in information coding remains an open question. Here, we report slow modulation of theta power and neuronal firing at a time scale of about 1 s, expressed in the rat hippocampus during both REM sleep and motor/cognitive behaviors. We show that second-order spectral analysis is relevant for decoding neuronal information on a slower time scale than usually assumed for brain rhythms.

RESULTS

Theta Power Slow Modulation (TPSM) as a "Second-Order" Oscillation

Recording spontaneous LFP and unit activity from the hippocampal CA1 pyramidal layer of freely behaving rats during various behavioral situations including REM sleep, open-field exploration and a protocol in which the animals were trained to alternatively run in a maze and in a wheel to get a reward (data recorded in and provided by the Buzsáki lab [Pastalkova et al., 2008]), we observed that theta oscillations were not stable in amplitude but rather increased and decreased on a reproducible time basis of about 1 s. Already visible in the raw (unfiltered) LFP traces, this theta power slow modulation (TPSM) is most striking in multitaper time-frequency spectrograms displaying the fluctuations of theta power over time (Figure 1A for sleep, Figure 1B for open-field, Figure 1C for maze, Figure 1D for wheel running). Because the modulation of an oscillation is not an LFP oscillation

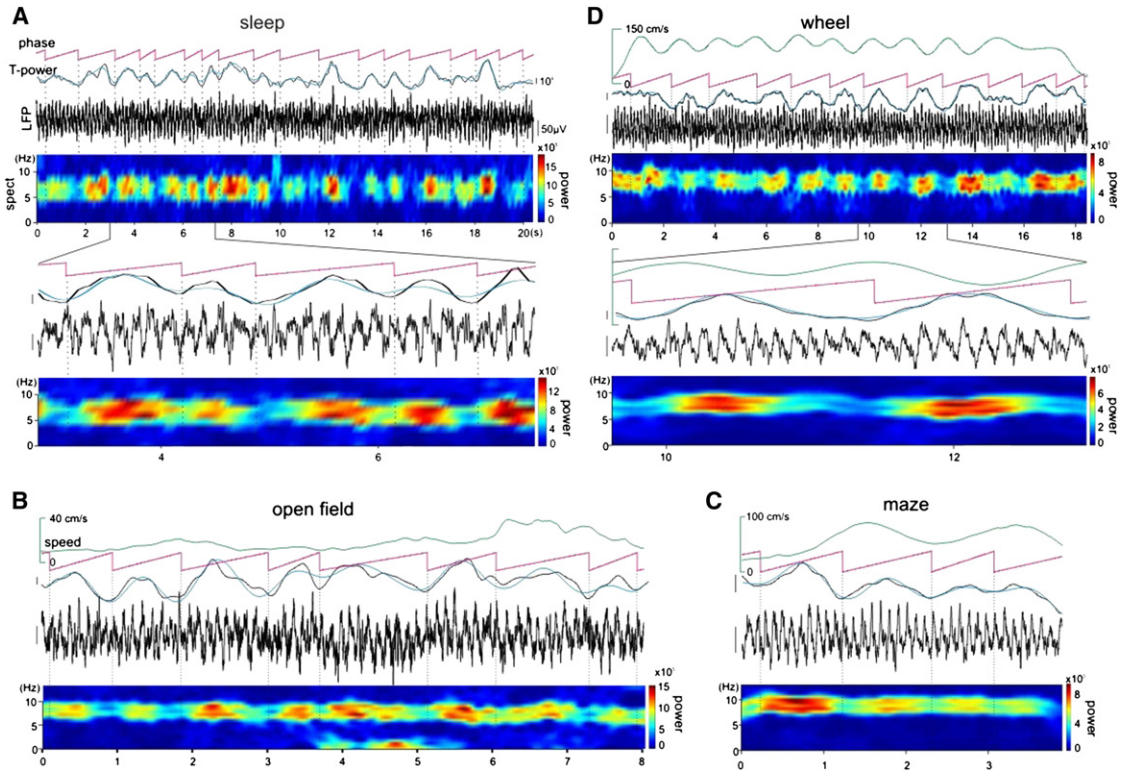

Figure 1. Theta Power Slow Modulation (TPSM) during REM Sleep, Open-Field Exploration, and Maze and Wheel Running

(A) Continuous time-frequency spectrogram (spect) of the LFP recorded from CA1 pyr layer during 20 s of REM sleep. Upper traces, corresponding wide-band EEG (black curve, LFP), superimposed instantaneous theta power (integrated in the 4–11 Hz band, black curve, T power) and filtered theta power (low-pass 1.8 Hz, blue curve); pink line, TPSM phase (from 0 to 2π, phase); dashed vertical lines indicate $0/2\pi$ phase of TPSM, corresponding to local theta power minima in the LFP and time-frequency spectrogram. Lower inset, 4.5 s of recording at expanded time scale.

(B) Same as in (A) but during open-field exploration. Top green line, instantaneous animal speed.

(C) Same as in (B) but during a maze-running sequence.

(D) Same as in (B) but during a continuous 18 s wheel running sequence. Lower inset, 3.5 s of recording at expanded time scale.

Note the fluctuations of theta power on a 1 s time scale in all four behaviors. See also Figure S7.

itself, its expression does not necessarily appear as a specific power peak in the "primary" power spectrum but can be identified in the second-order spectrum defined as the spectrum of the power fluctuations for a given frequency band (see Figure S1 available online). We therefore performed second-order spectral analysis (Drew et al., 2008) of LFP power in the integrated theta frequency band (4–11 Hz) and indeed observed the presence of a peak at 0.5–1 Hz, indicating robust expression of TPSM at this frequency in the tested behavioral conditions (Figure 2A for sleep, Figure 2B for open-field, Figure 2C for wheel running). These results were confirmed by additional analysis to exclude the possibility that the 0.5–1 Hz peak in the second-order theta power spectrograms might derive from smoothing of theta power in the 1 Hz range under the influence of the selected time window for theta power quantification. First, similar results were obtained using wavelet analysis to quantify instantaneous theta power (Figure S2). Second, we observed that the second-order theta power spectrum had a peak at the same frequency for varying multi-taper time-window sizes (range 0.6–1.6 s; Figure S2). For further analysis, we kept a window size of 1 s, yielding good peak-to-noise ratio (Figure S2). And third, a similar 0.5-1Hz peak was also observed in the spectrogram of theta power fluctuations measured as the peak-to-trough amplitude of each theta cycle in the filtered 2-30Hz EEG trace (Figures 2A–2C), excluding the potential interference with any filtering or smoothing of theta oscillations (4–11 Hz). Run durations in the maze (typically 3 to 5 s) were too short for spectral analysis below 0.5Hz with accuracy above 0.2 Hz, precluding reliable peak detection in the range 0.5–1 Hz. Nevertheless, the histogram of TPSM cycles durations shows a peak around 1 s, indicating a similar 0.5–1 Hz dominant frequency for TPSM in the maze (Figure 2D).

Endogenous Generation of Hippocampal TPSM

What is the relationship between TPSM and other factors known to modulate theta oscillations? It has been shown recently that in the behaving monkey auditory cortex (Lakatos et al., 2005), delta oscillations could modulate theta power. However, in our recordings, delta oscillations were typically expressed in the 2–4 Hz frequency range instead of 0.5–1 Hz for TPSM (Figure 3A, wheel). As illustrated in Table S1, we identified and compared the periods of TPSM and delta oscillations (delta power threshold,

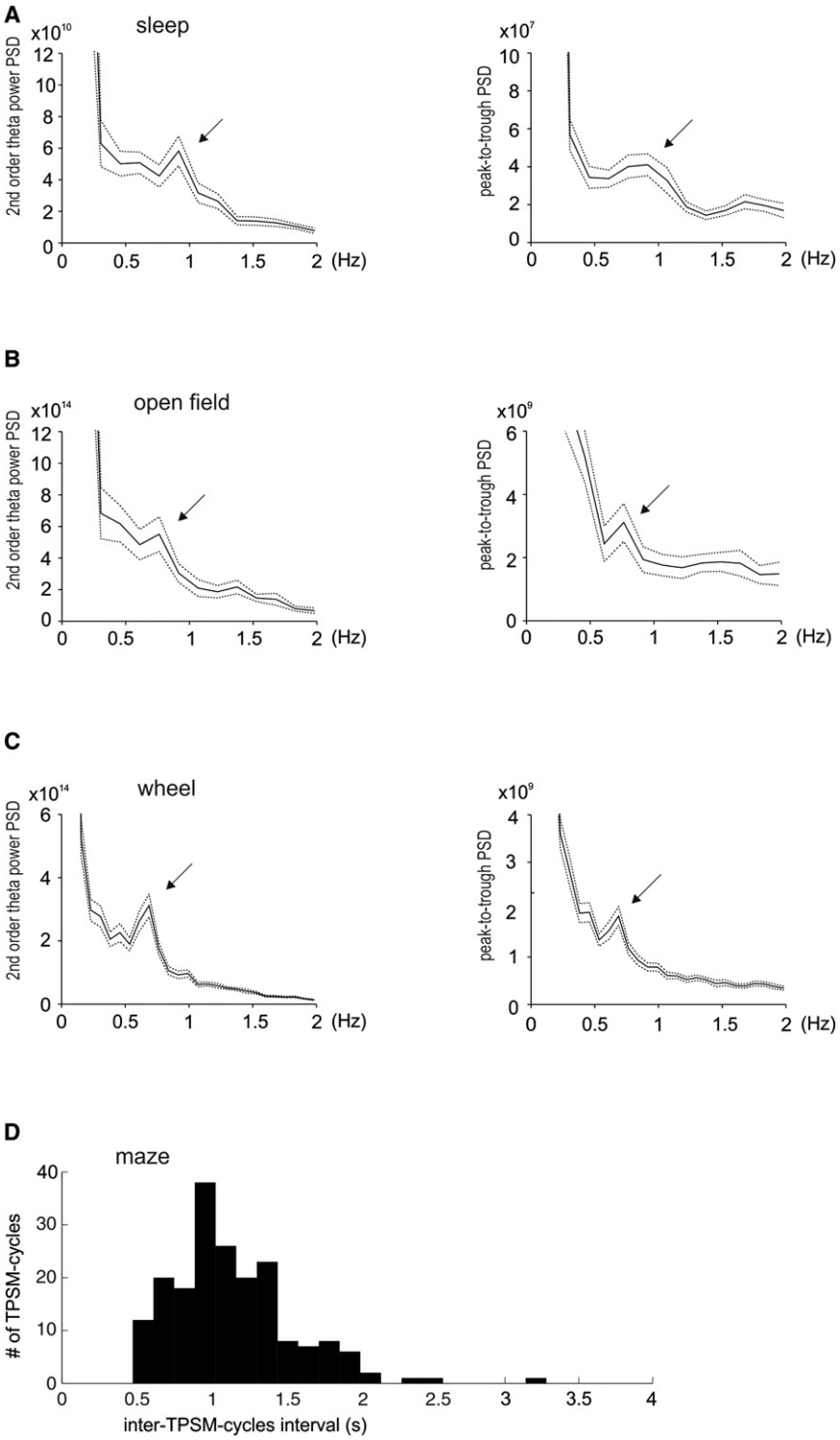

Figure 2. Preferred Modulation of Theta Power on the Second Time Scale

(A–C) Theta "second-order" power spectra (i.e., power density spectra [PSD] of spontaneous theta amplitude fluctuations) during REM sleep (A), open-field (B), and wheel (C) running. Left, PSD (mean ± SD) of the instantaneous theta power measured using the multitaper method. Right, PSD (mean ± SD) of the instantaneous theta amplitude measured as the peak-to-trough amplitude of each theta cycle from the 2–30 Hz band-pass-filtered LFP. Note the peak around 0.7 Hz in all conditions (arrow), corresponding to the preferred time scale of theta power slow modulation (TPSM).

(D) Histogram of inter-TPSM-peaks intervals in the maze.

See also Figure S1.

mean −0.1 SD) in each behavioral condition. During open field and wheel running, we observed that the proportion of TPSM time relative to total time was similar to its proportion relative to delta time, indicating that the expression of delta had no incidence on the expression of TPSM in these behavioral conditions, and vice versa. During sleep and running in the maze, expression of TPSM was significantly reduced during delta periods ($p < 0.05$; Table S1). Therefore, the periods with high delta power did not coincide with those of TPSM expression. Moreover, even when coexpressed, there was no correlation between the phases of delta and TPSM oscillations (Table S1). Altogether, these results suggest that TPSM is distinct from delta modulation of theta power.

Because previous observations suggested that theta power was correlated with running speed (Czurkó et al., 1999; DeCoteau et al., 2007; McFarland et al., 1975; Montgomery et al., 2009; Rivas et al., 1996; Shen et al., 1997; Whishaw and Vanderwolf, 1973), cyclic changes in theta power might result from systematic changes in running speed. Overall, we indeed observed that theta power globally correlated with running speed when selecting periods of several seconds with relatively constant running speed ($p < 0.05$, paired Student t test, open field, n = 9 sessions from 4 animals; maze, n = 10 sessions from 3 animals; wheel, n = 8 sessions from 3 animals; Figure 3A). But finer analysis considering instantaneous running speed at a time scale closer to that of theta oscillations (see Experimental Procedures) revealed no systematic correlation of running speed or acceleration with theta power ($p > 0.05$, Pearson linear correlation; Figure 3B) or TPSM phase ($p > 0.05$, circular-linear correlation analysis [Berens, 2009] and Rayleigh test; Figure 3C). This is most striking for maze/track recordings, in which although our results are in agreement with the recent report that globally

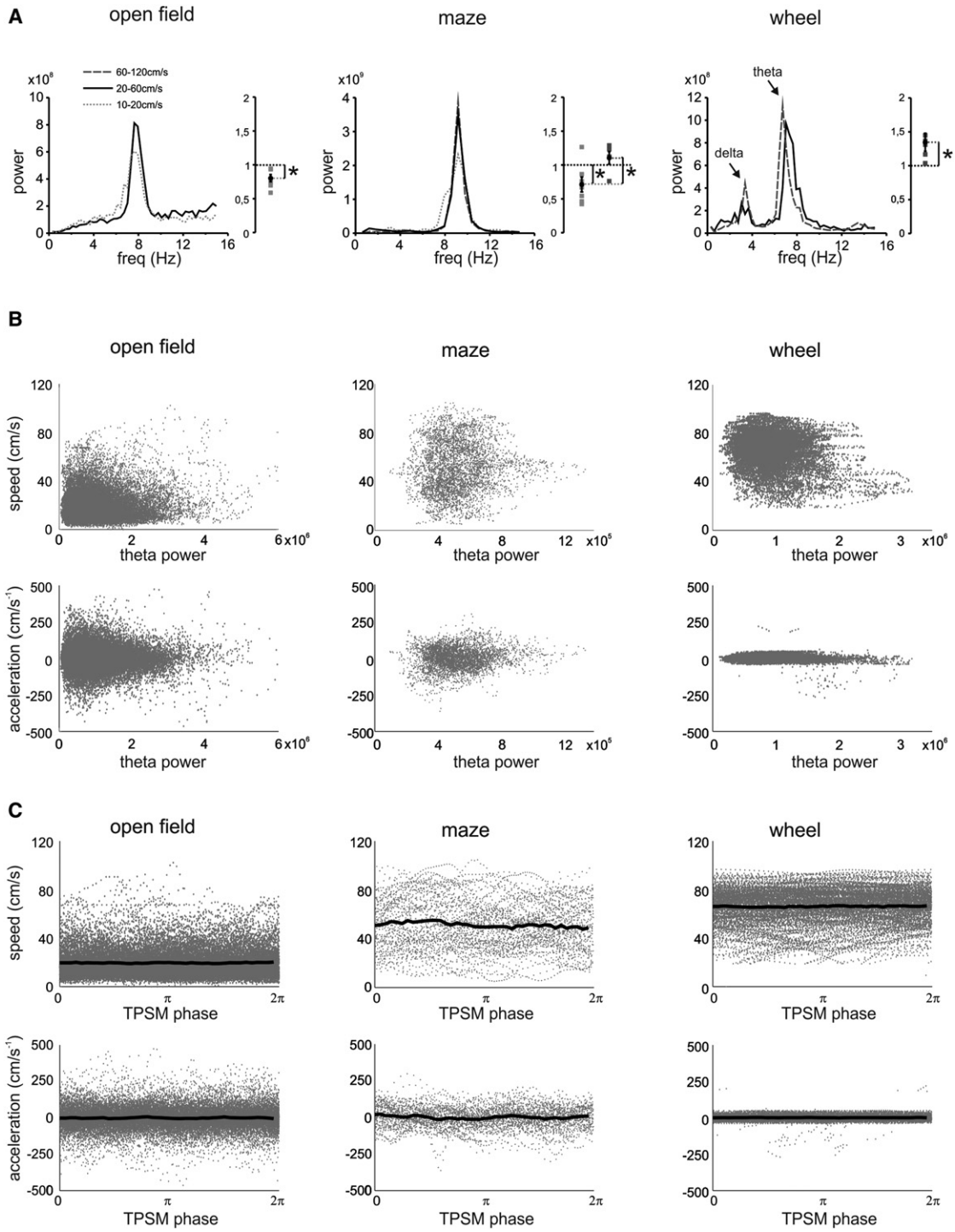

Figure 3. Global and Instantaneous Relationships between Theta Power Fluctuations, Running Speed, and Acceleration

(A) First-order power spectrum density (PSD) of raw EEG for continuous periods (mean period duration = 4.3 ± 0.07 s in open field, 4.1 ± 0.12 s in the maze, 14.7 ± 0.25 s in the wheel, n = respectively 435, 86, and 90 running periods) of different running speeds (10–20 cm/s, dotted light gray; 20–60 cm/s, black, 60–120 cm/s, dashed dark gray). For each behavioral condition (left, open field exploration; middle, maze; right, wheel running), PSD corresponding to one recording session, together with a summary histogram of the normalized (relative to values obtained for the 20–60 cm/s speed range) theta power peaks obtained from all recording sessions (open field, n = 9 sessions from 4 animals; maze, n = 10 sessions from 3 animals; wheel, n = 8 sessions from 3 animals, black squares with error bars indicate mean ± SEM; star, significant difference, Student's t test $p < 0.05$). The 60–120 cm/s range is not represented in the open field, nor does the 10–20 cm/s range in the wheel, because animals did not consistently run at those speeds during those tasks.

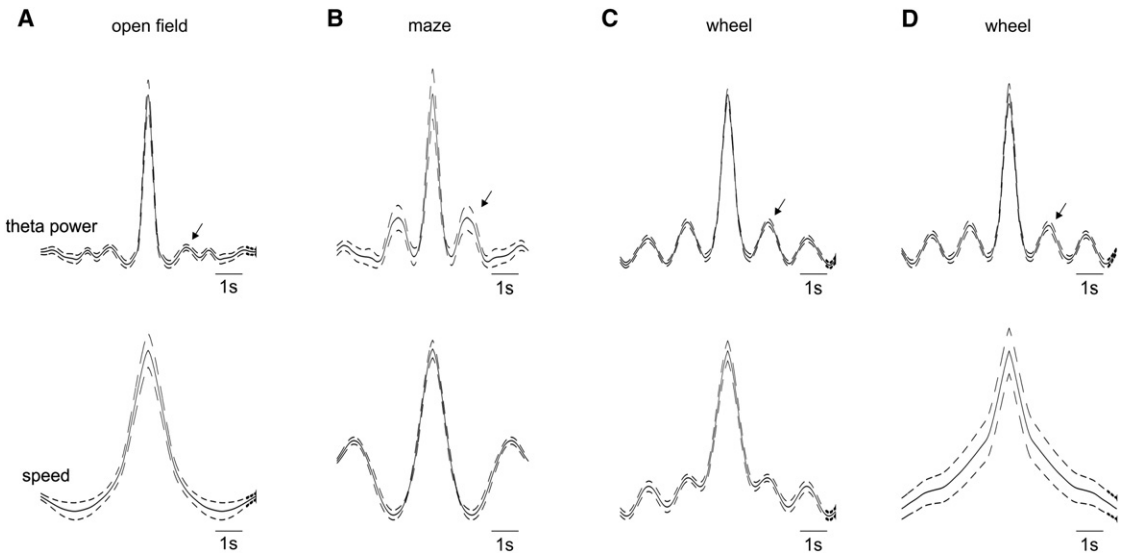

Figure 4. Distinct Fluctuations of Theta Power and Instantaneous Running Speed

Autocorrelation function (normalized) of MTM-theta power (upper traces, mean ± SD) and instantaneous speed (lower traces, mean ± SD) during open-field (A), maze (B), and wheel running (C and D).

(C) and (D) illustrate two different recording sessions from the same animal as in Figure 1D. Note the secondary bump around 1.5 s (arrow) in all conditions for MTM-theta power compared to the diversity of autocorrelation functions observed for speed.

faster runs were associated with larger average theta power estimated on a run per run basis (Hinman et al., 2011), visual inspection of theta power and running speed within individual runs clearly shows a lack of correlation between these two variables (in Figure 1C, instantaneous speed displays two clear cycles of fluctuation while TPSM shows 4 cycles during the same 4 s running period). More systematic comparison of speed and theta power autocorrelograms confirmed that even though both parameters can occasionally oscillate at similar frequency, they most often show pretty different profiles (Figure 4). Altogether, these results indicate that theta power modulation by running speed or acceleration does not account for TPSM.

During sleep, transient increases of theta power have been described as "phasic REM" sleep (Karashima et al., 2005; Montgomery et al., 2008; Sano et al., 1973). Sleep-related TPSM is rather related to tonic REM because (1) it was not associated with the increased theta frequency and the increased power of high-frequency components which accompany phasic REM, (2) it could occur in a continuous manner during several seconds, and (3) it was expressed throughout REM sleep (see Experimental Procedures; n = 4 animals), while phasic REM episodes typically last for about one second and represent around 4% of REM sleep (Montgomery et al., 2008). Because TPSM was observed in both running and sleeping behaviors and did not correlate with animal's speed or acceleration, we propose that it does not directly depend on motor behavior but is rather generated endogenously in the brain.

TPSM Phase-Locked Neuronal Firing

What is the physiological relevance of TPSM? More specifically, does it influence neuronal firing during sleep and awake behaviors? Analysis of population firing indicated significant ($p < 0.05$, Rayleigh test) but rather weak locking of CA1 pyramidal multinit activity to TPSM-phase in all behavioral conditions tested (modulation strength for sleep, $\kappa = 0.1 \pm 0.03$, n = 4/4 recording sessions from 4 animals; for open field, $\kappa = 0.07 \pm 0.01$, n = 8/9 recording sessions from four animals; for maze, $\kappa = 0.07 \pm 0.02$, n = 9/10 recording sessions from three animals; for wheel running, $\kappa = 0.05 \pm 0.004$, n = 10/10 recording sessions from three animals). Although no significant difference ($p > 0.05$, two sample t test) in preferred firing phase was observed between conditions (preferred firing phase for sleep, $\mu = 0.87 \pm 0.07\pi$; for open field, $\mu = 1.04 \pm 0.05\pi$; for maze, $\mu = 1.2 \pm 0.15\pi$; for wheel running, $\mu = 0.93 \pm 0.07\pi$), further investigation revealed a real diversity at the single cell level.

During sleep (Figure 5A), we found that 34% of the recorded neurons (47 out of 138, n = 4 animals) were significantly TPSM phase locked ($p < 0.05$, Rayleigh test) and displayed a preferred firing phase of 0.9π, nearly corresponding to the time of maximal theta power.

In the awake rat, there is a strong spatial correlate to hippocampal firing (Huxter et al., 2003, 2008; Jensen and Lisman, 2000; O'Keefe and Dostrovsky, 1971). For open field and maze running, we therefore focused our analysis on place cells (n = 123 neurons from 4 animals in open field, 264 neurons

Note increased theta power (7–11 Hz) during periods of increased running speed.

(B and C) Scatter plots showing theta power (B) and TPSM phase (C) versus instantaneous (1 point per tracking sample; black line, mean) speed (upper plots) or acceleration (lower plots) for one recording session during open -field (left), maze (middle), and wheel (right) running.

Note the poor correlation of theta power and TPSM phase with instantaneous speed and acceleration. See also Figure S2 and Table S1.

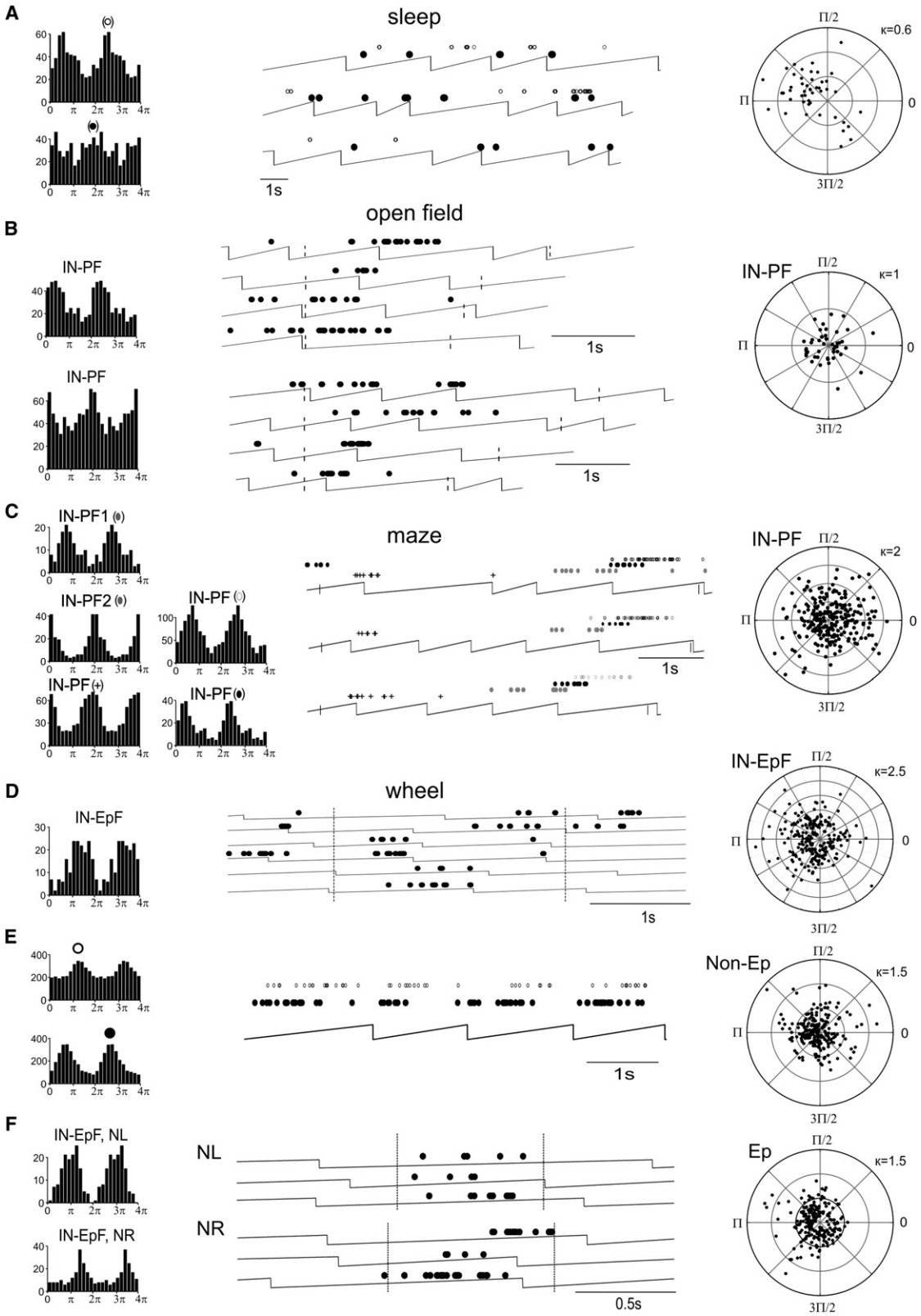

Figure 5. TPSM Phase Locking of Neuronal Firing

Histogram distributions (left) and raster plots (middle) showing spiking activity of individual cells (one symbol per neuron/place field) relative to the phase of TPSM. Broken line, TPSM phase from 0 to 2π; vertical dotted lines in (B) and (C), times of entry and exit in the corresponding cell's place field; vertical lines in (D) and (F),

from 3 animals in the maze) and examined separately the spikes discharged within (IN-PF) each neuron's place field. We observed significant ($p < 0.05$, Rayleigh test) TPSM-phase locking of IN-PF firing for 36% of place fields in open field (Figure 5B) and 72% of place fields during maze running (Figure 5C), with a higher diversity of preferred phases than during REM sleep (compare circular plots in Figure 5B [open field] and 5C [maze] to 5A [sleep]).

An interesting equivalent to the location-dependent firing of place cells is the time-dependent firing of "episode cells" reported by Pastalkova et al. (2008), a data set that we used for further analysis in the present study. While the animals were to run for a fixed amount of time in a wheel between successive maze runs, each moment in time (like each spatial position during spatial navigation) was characterized by the activity of a particular set of neurons, as members of self generated sequences of neuronal firing potentially encoding elapsed time during this fixed-delay period. As for place cells, we observed that the spikes discharged by 51% of episode cells (71 among 138 time-dependent firing cells) within their high-firing periods (i.e., within their episode field, IN-EpF) during wheel running trials displayed significant TPSM-phase locking (Figure 5D). Interestingly, some cells firing in a time-independent manner in the wheel (nonepisode cells) were also locked relative to TPSM phase (Figure 5E). Therefore, TPSM is robustly expressed during sleep and awake behaviors and neuronal firing is correlated with TPSM phase.

TPSM Supports Spatial and Temporal Coding in Open Field and Maze and Wheel Running

Although hippocampal place cells fire preferentially within specific locations, a significant proportion of their spikes is discharged outside of their place fields. Do the spikes fired by the same neuron inside (IN-PF) versus outside (OUT-PF) its place field show similar relationships with TPSM phase? If not, TPSM phase might help distinguish between IN-PF and OUT-PF spikes, information of high potential relevance for place coding.

In open field, we actually observed that 59% of TPSM-phase locked place cells displayed distinct phase relationship for IN-PF compared to OUT-PF spikes ($p < 0.05$, Kuiper test; Figure 6A). In order to quantify the corresponding gain of information provided by TPSM in the open field, we used a formula derived from the information theory (see Experimental Procedures) and previously used to estimate the spatial specificity (in bits per spike) of place firing (Markus et al., 1994). As illustrated in Figure 6B, taking TPSM phase into account to discriminate whether the animal is inside or outside the cell's place field increased information content by 26% ± 8% (initial mean information content = 0.49 ± 0.06 bits/spike, net gain from TPSM phase = 0.07 ± 0.015 bits/spike, $p < 0.05$ paired Student t test, n = 44 significantly TPSM phase-locked place cells). It has been reported that a significant proportion of place cells may have several place fields in the same environment (Dragoi et al., 2003; Leutgeb et al., 2007; Maurer et al., 2006). How efficient is TPSM in separating the distinct place fields of the same place cell? In open field, 27% of place cells had multiple place fields (n = 33/123 place cells). In 39% of these, the spikes fired by the same neuron within at least one of its place fields were significantly phase locked to TPSM ($p < 0.05$, Rayleigh test). Adapting the previous formula to quantify the potential contribution of TPSM in discriminating between the two place fields of the same place cell (see Experimental Procedures), we found a 52% ± 22% increase in information content (initial mean information content = 0.08 ± 0.02 bit/spike, net gain from TPSM phase = 0.06 ± 0.02 bit/spike, $p < 0.05$ paired Student t test, n = 13 TPSM phase-locked double-place-field cells, Figure 6B). As illustrated in Figure S5, our spike-sorting method makes it unlikely that these results were significantly affected by units misclassifications attributing the spikes fired by different neurons to the same cluster.

During maze running, animals ran repeatedly along the same path in a very stereotypic manner, and as illustrated in Figures 5C and 6C, striking examples of distinct place field spikes distribution relative to TPSM phase were observed. Among 348 place fields from 289 cells, 241 corresponded to single place fields and 107 belonged to cells having multiple place fields (37 double and 11 triple-place-field cells). In the maze, taking TPSM phase into account to discriminate between IN-PF and OUT-PF firing increased spatial information content by 62% ± 6% (initial mean information content = 0.55 ± 0.04 bit/spike, net gain from TPSM phase = 0.29 ± 0.03 bit/spike, $p < 0.05$ paired Student t test, n = 250 TPSM phase-locked place fields; Figure 6D). We ran statistical analysis and found that the spikes from 58% of all pairs of multiple place fields displayed different TPSM phase locking (among 96 pairs of multiple place fields, 56 were statistically different, Kuiper test, $p < 0.05$). Taking TPSM into account for discrimination of double place fields increased the information content by 72% ± 10% (initial mean

times of entry and exit in the corresponding cell's episode field. Polar plots (right), TPSM phase-locking parameters (von Mises parameters μ and κ, respectively representing preferred phase, plotted as polar coordinate, and strength of the modulation, plotted as distance from center) for each significantly (Rayleigh test, $p < 0.05$) modulated cell (sleep, 1 dot per cell, A), place field (open field and maze, 1 dot per PF, B and C), episode field (wheel episodes, 1 dot per EpF, D), and next-left/next-right running direction (directional wheel running, 1 dot per cell/next-left/next-right running direction, E and F).

(A) REM sleep, TPSM phase-locking of two distinct neurons (distinct colors).

(B) Open field, TPSM phase distribution of firing of two place cells (within-place-field spikes, IN-PF).

(C) Maze, TPSM phase distribution of within-place-field spikes (IN-PF) discharged by four distinct place cells (distinct symbols), one of which (filled gray circles) having two place fields (IN-PF1, IN-PF2).

(D) TPSM phase distribution of firing of a temporally selective (within episode-field spikes, IN-EpF) firing cell in the wheel.

(E) TPSM phase distribution of firing of two distinct nonepisode cells (distinct colors) in the wheel; right, corresponding polar plot (μ and κ) for all bidirectionally firing nonepisode cells (non-Ep).

(F) TPSM-phase distribution of IN-EpF spikes for a single episode cell during wheel running as a function of future running direction in the maze (NL, next-left; NR, next-right); right, corresponding polar plot (μ and κ) for all bidirectionally firing episode cells (Ep).

See also Figure S6.

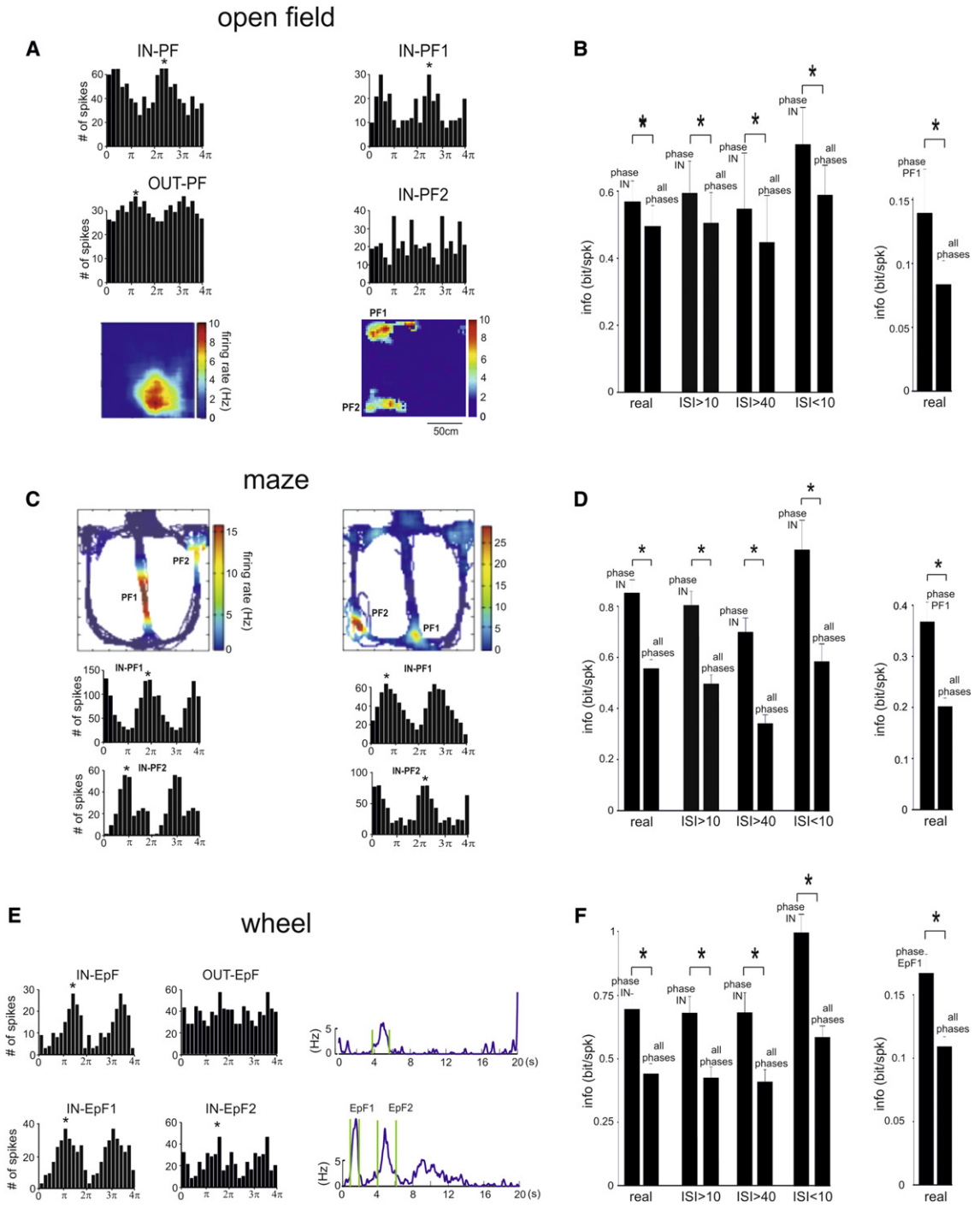

Figure 6. TPSM-Related Increase in Neuronal Information Content in the Open Field, Maze, and Wheel

(A) Left, TPSM phase distribution histograms of within-place-field (IN-PF) and out-of-place-field (OUT-PF) spikes for the same neuron (star, significant phase locking, $p < 0.05$, Rayleigh test). Below, firing-rate map showing the spatial distribution of the cell's firing. Note significant but distinct TPSM phase spikes distributions for IN-PF versus OUT-PF. Right, TPSM-phase distribution histograms of spikes discharged by a double place-field neuron in each of its place fields (IN-PF1 versus IN-PF2). Below, corresponding firing-rate map. Note distinct TPSM-phase spikes distributions for IN-PF1 versus IN-PF2.

(B) Left, information content (discrimination between IN-PF and OUT-PF in the open field, in bit/spike, mean ± SEM) of hippocampal place cells for spikes fired at the preferred IN-PF TPSM-phase (phase IN) compared to the same number of spikes fired at all other TPSM-phases (all phases). Real, analysis of the original spike train; ISI > 10, similar analysis except all bursts and spikes fired at high-frequency were omitted (all spikes with previous ISI < 10 ms omitted from analysis); ISI > 40, only spikes fired at less than 25 Hz (spikes with next ISI < 40 ms omitted from analysis); ISI < 10, only spikes belonging to bursts and high firing rate (all spikes with next ISI > 10 ms omitted from analysis). Right, information content for cells having multiple place fields (discrimination between IN-PF1 and IN-PF2,

information content = 0.2 ± 0.02 bit/spike, net gain from TPSM phase = 0.17 ± 0.03 bit/spike, $p < 0.05$ paired Student t test, n = 94 TPSM-phase-locked place-field pairs; Figure 6D).

Similarly in the wheel, 65% of episode fields were significantly associated with specific TPSM phase (Figures 5D and 6E), and TPSM increased the discrimination information content for IN versus OUT EpF by 92% ± 6% (initial mean information content = 0.44 ± 0.0 bit/spike, net gain from TPSM phase = 0.26 ± 0.02 bit/spike, $p < 0.05$, paired Student t test, n = 231 TPSM-phase-locked episode-fields; Figure 6F). Like place cells, 40% of episode cells had multiple episode fields, and taking TPSM into account increased episode fields discrimination information by 64% ± 9% (initial mean information content = 0.11 ± 0.01 bit/spike, net gain from TPSM phase = 0.06 ± 0.01 bit/spike, $p < 0.05$ paired Student t test, n = 177 TPSM phase-locked episode-field pairs; Figure 6F).

Considering the robust consistency in information gain, we propose that TPSM has the potential to significantly increase spatial (and time-related) information content and disambiguate between the multiple place fields (and episode fields) of the same cell.

TPSM Relationships with Time and Space

Searching for potential mechanisms that could account for location-dependent (i.e., IN-PF spikes) phase locking of spikes to TPSM, we considered the possibility for a correlation between firing rate or discharge mode (bursts instead of single spikes) and TPSM phase. If for example a neuron would discharge at different TPSM phases as a function of its firing rate (or mode), one might expect that IN-PF firing would be preferentially locked to TPSM phases related to high firing rates (or bursts) while OUT-PF firing would preferentially occur on TPSM phases related to lower firing rates. In order to control for the effects of firing rate on additional spatial information potentially provided by TPSM phase, we neutralized firing rate dynamics by computing the spatial-information index separately for various firing rates and discharge modes (see Supplemental Experimental Procedures). As illustrated in Figure 6 and Table S2, taking TPSM-phase into account to discriminate between IN-PF and OUT-PF firing (IN versus OUT EpF in the wheel) still provided significant increase in spatial information content when bursts (taken as successive spikes separated by less than 10 ms) were omitted from the original spike train, as well as when only spikes emitted at high frequency (ISI < 10 ms) or on the contrary at frequencies lower than 25 Hz (ISI > 40 ms) were taken into account. These results suggest that a direct relationship between firing rate and TPSM-phase is unlikely to account for the observed TPSM phase-related gain of spatial information.

Another possibility is that of a location-dependent modulation of theta power itself. For example, if theta amplitude was systematically maximal within a given place field area, the spikes discharged within this place field would likely be biased toward the corresponding phase of TPSM (i.e., π, for maximal theta power). We therefore computed signal-phase histograms corresponding to the TPSM phases expressed in each place field (i.e., distribution of LFP TPSM-phase relative to physical space; see Experimental Procedures). Although in the open field a significant signal modulation relative to TPSM phase was observed in 41% of TPSM phase-locked place fields (18 place fields among 44 whose IN-PF spikes were significantly phase locked to TPSM; Rayleigh test, $p < 0.05$; Figure 7A), it was most often (13 among 18 place fields) significantly different ($p < 0.05$, Kuiper test) from the distribution of IN-PF spikes relative to TPSM phase. This observation suggests that the TPSM phase-locking of spikes inside a place field cannot be explained by the preferred TPSM phase of the signal within this same place field.

A different situation prevailed in the maze in which, as expected from classical track running experiments, running was accompanied by a highly reproducible sequence of place cells firing, along with the animal's stereotypical spatial progression (Pastalkova et al., 2008). As observed in Figures 7B–7D and S3, TPSM was remarkably conserved from one run to the other, as was the motor behavior of the animal. Accordingly, we observed that TPSM was in fact phase locked to the environment (Figures 7B–7E), in accordance with a recent study reporting a strong correlation between theta power and animal's position in a maze (Montgomery et al., 2009). As a result, the relationship between IN-PF spikes and TPSM phase in the maze appears to be tightly related to the coincidence of place field position and phase locking of TPSM to space (Figures 6C and 7C–7E).

in bit/spike, mean ± SEM) for spikes fired at the preferred IN-PF1 TPSM-phase (phase PF1) compared to the same number of spikes fired at all other TPSM-phases (all phases). Star, significantly different, paired Student t test, $p < 0.05$.

(C) Two examples (left and right, two different place-cells in the maze) of TPSM-phase distribution histograms of spikes fired in one or the other place-field (IN-PF1 / IN-PF2) of the same neuron (top, corresponding firing-rate map). Note distinct TPSM-phase spikes distributions in each place field.

(D) Left, information content (discrimination between IN-PF and OUT-PF in the maze, in bit/spike, mean ± SEM) of spikes fired at the preferred IN-PF TPSM-phase (phase IN) compared to the same number of spikes fired at all other TPSM-phases (all phases). Real, analysis of the original spike train; ISI > 10, all spikes with previous ISI < 10 ms omitted from analysis; ISI > 40, spikes with next ISI < 40 ms omitted from analysis; ISI < 10, all spikes with next ISI > 10 ms omitted from analysis. Star, significantly different, paired Student's t test, $p < 0.05$. Right, information content (discrimination between IN-PF1 and IN-PF2, in bit/spike, mean ± SEM) for spikes fired at the preferred IN-PF1 TPSM phase (phase PF1) compared to the same number of spikes fired at all other TPSM phases (all phases). Star, significantly different, paired Student t test, $p < 0.05$.

(E) Upper, TPSM phase distribution histograms of within-episode-field (IN-EpF) and out-of-episode-field (OUT-EpF) spikes for an individual episode cell. Right, corresponding firing-rate versus time (vertical green lines, episode-field limits). Below, TPSM-phase distribution histograms of spikes discharged by another individual neuron in two distinct episode fields (IN-EpF1 versus IN-EpF2). Right, corresponding firing-rate versus time.

(F) Information content (left, discrimination between IN-EpF and OUT-EpF, right, discrimination between IN-EpF1 and IN-EpF2 in bit/spike, mean ± SEM) of hippocampal wheel cells for spikes fired at the preferred IN/OUT-EpF (left) or IN-EpF1/IN-EpF2 (right) TPSM-phase (phase IN) compared to the same number of spikes fired at all other TPSM phases (all phases). Real, analysis of the original spike train; ISI > 10, all spikes with previous ISI < 10 ms omitted from analysis; ISI > 40, spikes with next ISI < 40 ms omitted from analysis; ISI < 10, all spikes with next ISI > 10 ms omitted from analysis. Star, significantly different, paired Student's t test, $p < 0.05$.

See also Figure S5.

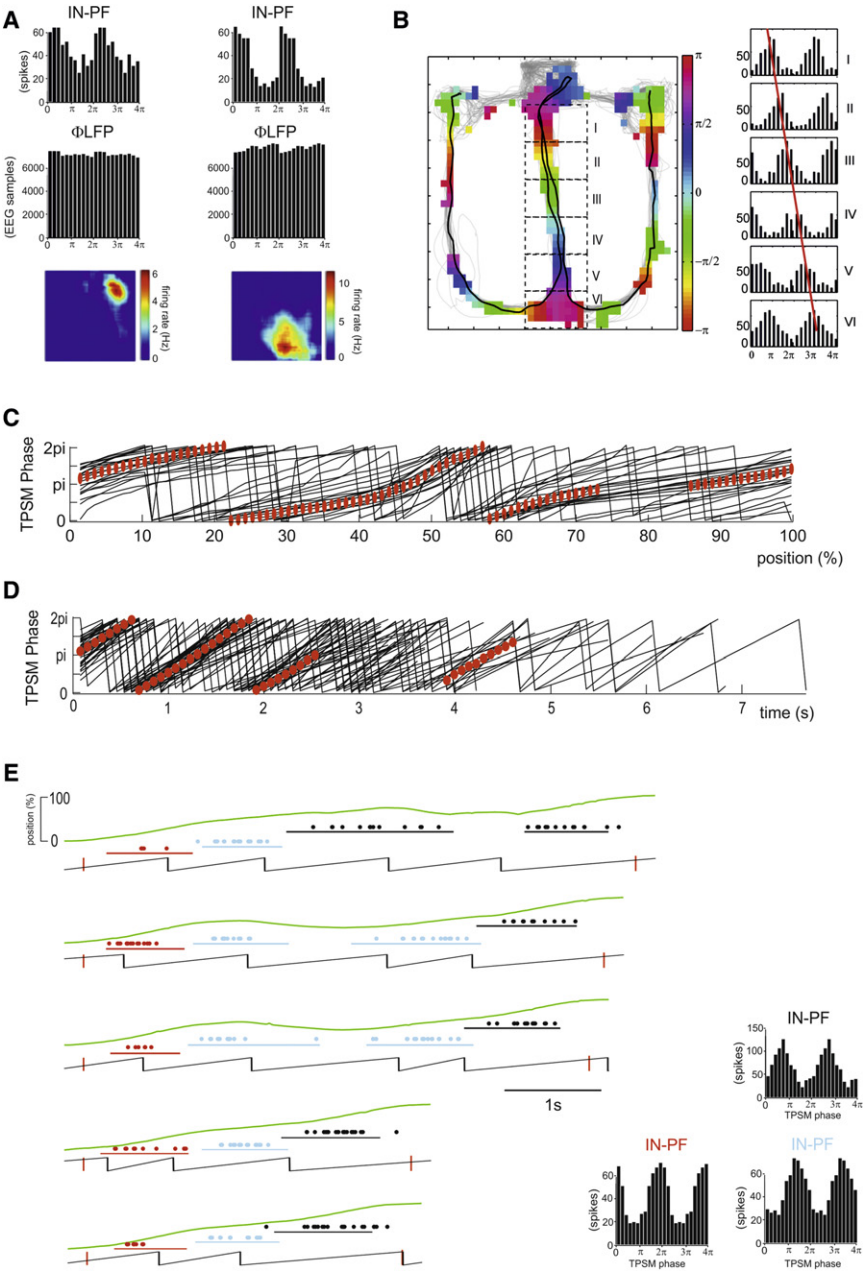

Figure 7. TPSM Relationships with Time and Space

(A) TPSM phase distribution histograms of within-place-field spikes (IN-PF) and signal (Φ [LFP]) for two different neurons in the open field. Φ (LFP) histograms correspond to the TPSM-phase distribution of all time points (sampling rate 1,250 Hz) during which the animal was located within the PF, while IN-PF histograms correspond to the TPSM phase distribution of IN-PF spike times. Bottom, firing-rate maps showing the corresponding neuron's place fields. Note distinct TPSM-phase modulation of IN-PF versus signal.

(B) TPSM phase map (color-coded mean TPSM phase): each space bin (successive rat positions) is color coded, showing the average TPSM-phase at this location. Gray lines, all trajectories of the recording session. Black lines, examples of two individual trajectories from the wheel (top, middle) to the left and right reward ports of the maze (top, left and right extremities). Right, histogram distribution of TPSM phases (one value per space bin per animal run) at the corresponding locations in the maze (box areas I to VI of the central arm of the maze, as indicated in the TPSM phase map on the left). Note TPSM phase locking on the physical environment.

(C) Instantaneous TPSM phase as a function of position (normalized, from start to reward location) in the maze. Broken lines, superimposed individual runs. Red dots, mean TPSM phase (μ von Mises parameter) computed from all individual runs for each position and displayed only when significant (Rayleigh test, $p < 0.05$).

(D) Instantaneous TPSM-phase as a function of time in the maze (from start to reward location). Broken lines, superimposed individual runs. Red dots, mean TPSM phase (μ von Mises parameter) computed from all individual runs for each time point and displayed only when significant (Rayleigh test, $p < 0.05$).

(E) Raster plots and corresponding TPSM spike-phase histograms (right corner) for three individual neurons (one color/neuron) during five individual runs in the maze, showing their firing (one dot per spike) as a function of time (vertical red lines, start and end times of the run), TPSM phase (broken line, from 0 to 2π), and position (green curve, normalized position in the maze; horizontal colored lines, animal within the corresponding color-coded cell's place field). Note similar TPSM-phase locking during fast and slow runs. The red and black cells are the same as in Figure 4C.

See also Figure S3 and Table S2.

To further investigate the potential relative influences of time and space on hippocampal activity, we examined TPSM during wheel running, in which although the animal is running, its spatial location does not change (Czurkó et al., 1999; Pastalkova et al., 2008). As in the maze, we observed that TPSM-phase was a consistent function of time across trials during wheel running (Figures 8A and S4). Most striking in the initial few seconds of the run (Figure S3C), this relationship still held after 20 s of running time (Figure S3D), suggesting that during stereotypic behavior, theta power fluctuations can be significantly conserved over extended periods of time (>10 s).

TPSM Supports Prospective/Retrospective Behavioral Coding in Wheel Running

A recent study based on the same data set suggested that firing of a subset of hippocampal pyramidal cells during wheel running might relate to past or future behavior of the animal (Pastalkova et al., 2008). We therefore asked whether TPSM might also

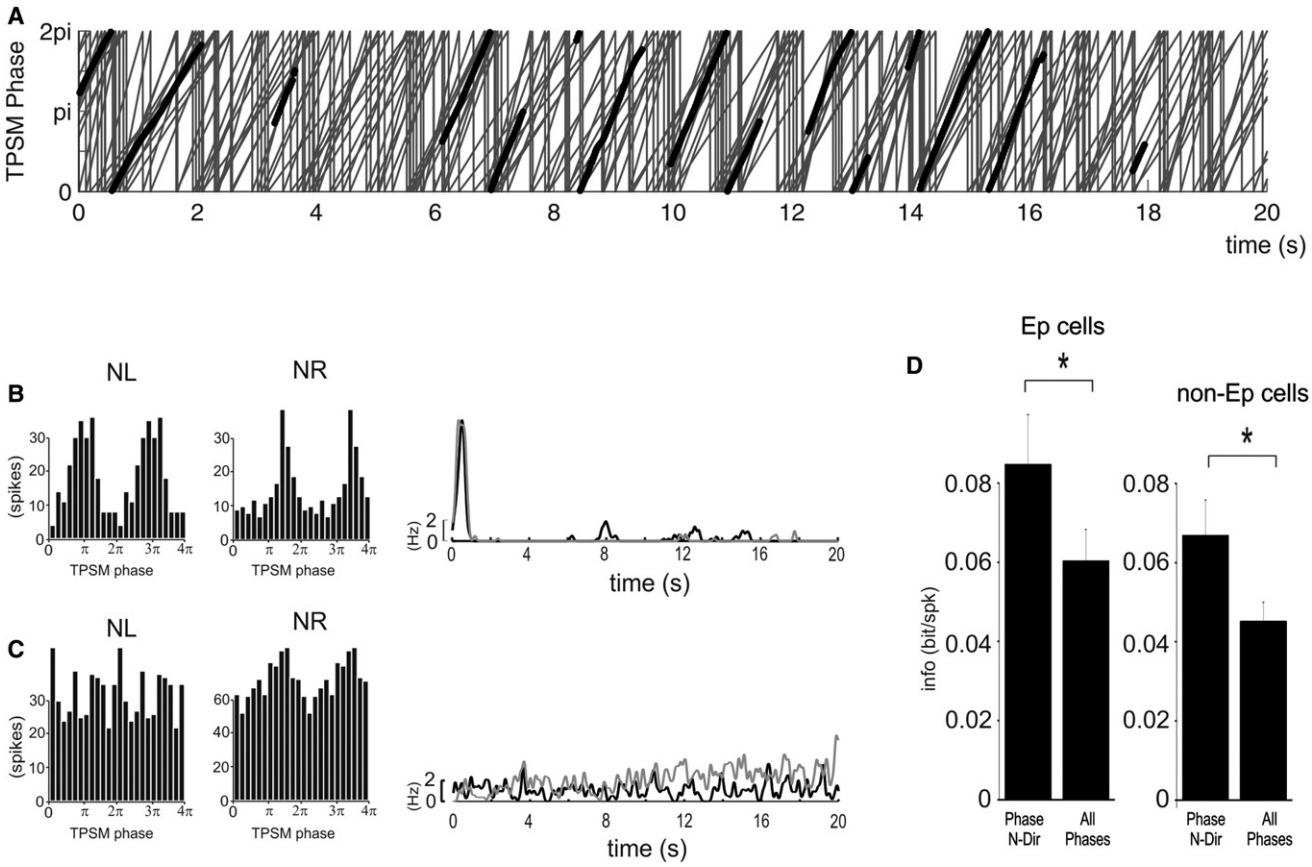

Figure 8. TPSM-Related Increase in Prospective/Retrospective Neuronal Information Content in the Wheel

(A) Instantaneous TPSM phase as a function of time in the wheel. Broken gray lines, superimposed individual runs. Black dots, mean TPSM phase (μ von Mises parameter), computed from all individual runs for each time point and displayed only when significant (Rayleigh test, $p < 0.05$).

(B and C) TPSM phase distribution histograms of spikes discharged in the wheel by individual neurons (B, an episode cell; C, a nonepisode cell) in runs preceding left (NL, next-left), or right (NR, next-right) maze runs. Right, corresponding firing-rate versus time (gray, NL; black, NR).

(D) Information content (discrimination between NL and NR, left Ep-cells, right, non-Ep-cells, in bit/spike, mean ± SEM) of hippocampal wheel cells for spikes fired at the preferred directional NL/NR TPSM-phase (phase N-Dir) compared to the same number of spikes fired at all other TPSM phases (all phases). Star, significantly different, paired Student's t test, $p < 0.05$.

See also Figure S4.

participate in time-related information coding. In this behavioral protocol, wheel runs were associated with an alternation maze running task, meaning that individual wheel runs could all be classified as either next-left or next-right runs, depending on whether the animal was to go to the left or right arm of the maze to get a reward (see Experimental Procedures). We tested the influence of TPSM on neuronal firing in both next-left/next-right conditions and observed that among 588 "bidirectional" cells that fired in both next-left and next-right runs, 325 (55%) were significantly locked to TPSM phase (Figures 8B and 8C). In fact, taking TPSM into account for discrimination of next-left versus next-right runs increased the information content in both episode and nonepisode bidirectional firing cells by respectively 43% ± 8% and 51% ± 10% (episode cells, initial mean information content = 0.06 ± 0.01 bit/spike, net gain from TPSM phase = 0.02 ± 0.01 bit/spike, n = 150 cells, $p < 0.05$, paired Student t test; nonepisode cells, initial mean information content = 0.05 ± 0.005 bit/spike, net gain from TPSM phase = 0.02 ± 0.01 bit/spike, n = 175 cells, $p < 0.05$, paired Student t test; Figure 8D). Therefore, while running in the wheel (present behavioral action), the firing phase (relative to TPSM) of some neurons is indicative of the past/future running direction of the animal (i.e., some neurons fire on different TPSM phases in the wheel depending on whether the animal is coming from the right arm and going next to the left arm, or on the contrary coming from the left arm and going next to the right arm). Even though future and past are ambiguously combined in the wheel-maze running task because the animal is alternating between left and right turns (a future left-arm run corresponds to a preceding right-arm run), our results indicate that TPSM phase locking of hippocampal cells' firing can also relate to the internal representation of events out of the present time such as past/future running trajectory (i.e., prospective/retrospective behavioral information encoding).

DISCUSSION

The presence of oscillatory components within brain electrical activity is often investigated using Fourier analysis-based spectral decomposition of signal power, which provides an estimate of the average amplitude of signal fluctuations at each frequency. However, as illustrated in our simulated signal made of a rhythmically modulated theta oscillation, periodic waxing and waning of theta oscillations is not revealed by simple power-spectral analysis. To overcome this limitation, we analyzed theta power fluctuations using second-order analysis (Drew et al., 2008), which consists of power-spectral decomposition of the fluctuation of theta amplitude over time. This revealed the presence of robust rhythmic fluctuations of theta power (TPSM) on a time scale of about 1.3 s, expressed in REM sleep, open-field exploration, and wheel and maze running. Therefore, theta power fluctuates in a rhythmic manner at about 0.7 Hz during a variety of behavioral situations, suggesting that TPSM is a general phenomenon.

In signal theory, both the product of a carrier wave (in our case, theta) and a modulating slow wave, or the interference between two summed theta waves of slightly different frequencies, would result in a rhythmically modulated theta wave, similar to TPSM (Khanna and Teich, 1989; O'Keefe and Recce, 1993). Both hypotheses, which are not mutually exclusive, are compatible with our present knowledge of brain physiology. First, modulation of theta amplitude by slower (i.e., delta, 1.5–3 Hz) oscillations has been observed in the awake monkey primary auditory cortex (Lakatos et al., 2005). In the present study, the 1 Hz high-pass filter we used to prevent signal offset and maximize amplitude resolution would make the identification of a primary slow oscillation in the infra-Hertz range potentially unreliable. Therefore, although the periods and frequencies of TPSM and hippocampal delta oscillations did not match in our recordings, the possibility remains that theta power might be modulated by an underlying slow wave. Second, previous studies reported two types of theta oscillations in the hippocampus, an atropine-resistant and urethane-sensitive type 1 theta related to voluntary movement and an atropine-sensitive, urethane-resistant type 2 theta possibly related to hippocampal-dependent sensory integration (Bland and Oddie, 2001; Kramis et al., 1975; Lee et al., 1994; Leung, 1984a, 1984b; Robinson et al., 1977; Sainsbury et al., 1987a, 1987b; Sutherland et al., 1982; Vanderwolf, 1969; Whishaw and Dyck, 1984). Because type 2 theta has a slightly slower frequency than type 1 theta (4–9 Hz against 6–12 Hz) (Kramis et al., 1975), their expected coexpression during behavior is also a potential source of oscillatory interference and TPSM generation. Further experimental work will be necessary to identify the precise mechanisms of TPSM generation.

It is widely assumed that theta power reflects the expression of sensory-motor integration underlying decisional and voluntary motor processes, so that a main function of theta would be to prepare and control relevant motor behavior (Bland and Oddie, 2001; Whishaw and Dyck, 1984). Our observation that changes in theta power occur in a cyclic manner during a whole variety of behaviors is therefore intriguing. It might suggest that the rat's behavior is controlled or updated on a predefined time schedule. In the maze, it is ambiguous whether theta power fluctuations occurring at specific time points and locations are due to intrinsic or external, behaviorally driven factors because of the stereotypic behavior of the animal in this task, generating confounding correlations among time, space, and behavior (such as the animal systematically initiating movement at the start location, turning at the T junction, slowing down before turn and reward locations). But on the other hand, TPSM was also robustly expressed in situations in which animals are not expected to follow stereotypic trajectories (open field) or were steadily running for several seconds without interruption (wheel), as well as in REM sleep during which the absence of sensory-motor and behavior-related processing favors the expression of endogenously generated brain patterns. Altogether, these results represent strong evidence for the presence of an endogenous rhythmic modulation of theta power in the hippocampal circuit, potentially reflecting the temporal organization of sensory-motor processes. While similarities between awake and REM-sleep theta activity have been proposed to result from the replay of awake activity during sleep (Louie and Wilson, 2001), the alternative hypothesis that endogenously generated sequences of activity might be played again during awake behavior (preplay) has recently received experimental support (Dragoi and Tonegawa, 2011). A daring hypothesis is therefore that awake theta power fluctuations and their behavioral correlates are influenced by rhythmic cycles of brain activity in the 0.5–1 Hz range, the endogenous nature of which is suggested by their expression during sleep, in absence of ongoing behavior. Further work will be necessary to decipher the relative influences of endogenous and external factors in the modulation of theta power and behavior.

Recording the EEG and neuronal discharge of multiple individually identified hippocampal neurons, we have observed that the endogenous, rhythmic fluctuations of theta power, also provided a temporal reference for neuronal population firing on a time scale of about 1.3 s. During sleep, most modulated neurons displayed a marked preference for the TPSM phase corresponding to maximal theta power. However, in contrast with this "default state," TPSM-phase locked neurons displayed a real diversity of preferred firing phases during awake behavior, a prerequisite for TPSM to serve as a substrate for information coding. Indeed, we observed that taking into account the TPSM phase at which each spike occurred improved the discrimination between the spikes fired by a neuron within versus outside its place field, between the spikes belonging to one or the other place field of neurons having multiple place fields, and between the firing that preceded alternating running directions after wheel running. Compared to maze experiments in which TPSM-phase preference of place-field spikes (and related spatial information content) was likely reinforced by the spatial coincidence of place-field location and TPSM phase-locking to space, wheel data allowed to dissociate the space and time correlates of TPSM and extend our conclusions from the spatial (place fields) to the temporal (episode fields) domain. Moreover, in the maze compared to the open-field, tighter coordination between motor behavior (spatial progression), global cortical activity pattern (TPSM), and neuronal firing (place cells firing) were associated with more precisely defined place fields and more efficient TPSM-related improvement of spatial information content of

individual place cells firing. We speculate that familiar and repetitive tasks such as maze running allow for stable coordination of various behavioral and neuronal components, resulting in more robust information coding so that the task can be performed more accurately and require less mobilization of attention. While previous reports have mainly considered theta power modulation as fluctuations of brain state or attention level, our results provide the first demonstration that theta power modulation might be used as a carrier for present and prospective/retrospective behavioral information encoding.

EXPERIMENTAL PROCEDURES

Electrophysiological Recordings

Eight male Long-Evans rats (300–500 g) were implanted with either eight movable tetrodes or with multisite silicon probes (Neuronexus, 32 and/or 64 sites, 4 or 8 shanks 200 μm apart, 8 recording sites per shank, 20 μm spacing between the sites), and neuronal activity was recorded (1,000× amplification, 1–9,000 Hz band-pass, digitized with 16 bit resolution, 20 kHz sampling rate using DataMax system, RC-electronics, Santa Barbara, CA) during different behaviors (sleep, open field, maze and wheel running). Localization of electrodes was histologically confirmed to be the CA1 pyramidal layer. One or two LEDs attached to the headstage were used to track the position of the animal (40 images per second) during open-field exploration of a large square box (120 × 120 cm, 50 cm high) or during running in a maze (100 × 120 cm) for water reward, the animals being trained to alternate between the left and right arms of the maze, and successive maze runs being separated by a wheel run of 10 to 20 s (cf Pastalkova et al. (2008) for a more complete description of this data set). Animal experiments were performed following INSERM guidelines and the official French veterinary regulation concerning animal experimentation (decret 87-848, 10/19/1987). All protocols were approved by the Institutional Animal Care and Use Committee of Rutgers University. Running speed was calculated as the distance between positions at 100 ms time intervals and averaged over ±100 ms around each time point. For PSD versus running speed analysis (Figure 3A), additional 800 ms smoothing was used to select periods in which running speed globally remained within specified ranges (10–20, 20–60, or 60–120 cm/s) for several seconds (at least 3 s in open field and maze, 10 s during wheel running). Spike sorting was performed by a semiautomatic clustering procedure (see Supplemental Experimental Procedures and Figure S5), yielding a total of 140 active pyramidal neurons during sleep (n = 4 animals), 573 in the maze (n = 3 animals), 569 during wheel running (n = 3 animals) and 193 in the open field (n = 4 animals).

Place and Episode Fields Definition

The determination of place fields was basically performed as in Leutgeb et al. (2007). For each cell, spatial distributions of firing rates (ratio of total number of spikes to occupancy duration in a given spatial bin) during locomotion (>5 cm/s) were calculated for each bin of the environment (50 × 50 bins) and then boxcar-averaged over the 25 neighboring bins (instead of a Gaussian kernel). Place fields included the bins with the highest firing rates (at least 2 Hz) and all contiguous bins in which the firing rate exceeded 20% of the peak firing rate. Place fields smaller than 16 bins or larger than half the environment were discarded. Episode fields (EpF) in the wheel were defined as periods <3 s with peak firing rate >5 Hz and 4SD above mean firing rate, EpF limits were set at 10% of the peak firing rate, as described in Pastalkova et al. (2008).

Theta Power Slow Modulation Analysis

Because theta is reliably expressed when the animal is moving, we have selected for analysis all awake periods with running speed >10 cm/s (although including brief interruptions of less than 200 ms). REM sleep periods were determined from manual threshold on theta/delta ratio, which provides a well contrasted estimation of REM sleep versus slow-wave state (Figure S6). Periods shorter than 3.5 s were discarded.

Time-frequency spectrograms of continuous LFP traces (EEG, sampling rate 1.25 kHz, hardware high-pass filter 1 Hz) were computed by using the multitaper method (1 s time window and 4 tapers) from the Chronux toolbox (Mitra and Bokil, 2008; http://chronux.org/). Theta power signal was measured from the raw EEG trace as the integrated power in the 4–11 Hz frequency band by using the multitaper method. For second-order analysis, theta power was also measured as the peak-to-trough amplitude of individual theta cycles in the 2–30 Hz filtered ("raw theta") EEG trace or by using Morlet-based wavelet analysis (Bruns, 2004). These methods yielded similar results (Figures 2, S2, and S6).

Local maxima (peaks) and minima (troughs) of theta power were detected and measured on the theta power trace, within 200 ms of the peaks and troughs obtained from the low-pass filtered theta power signal (fourth-order Chebychev, cutoff 1.8 Hz; Figure S7). TPSM cycles were defined as the intervals between successive theta power minima and a linear phase (from 0 to 2π) was defined between the successive troughs of TPSM cycles (see Supplemental Experimental Procedures). Results proved consistent using different thresholds for TPSM amplitude, taken as the TPSM-cycle-by-cycle difference between minimal and maximal values of theta power. Nevertheless, analyzed REM sleep periods are based on an automatic threshold at mean ± 0.7 SD of TPSM amplitude, which provided the best results (Figure S6).

"Second-order" power spectrum of the integrated theta power was computed on TPSM periods. In order to have a minimum frequency resolution of 0.1 Hz, TPSM periods shorter than 10 s were discarded.

Physiological Correlates of TPSM Phase

Spike-phase histograms represent the distribution of spikes relative to TPSM phase. IN-PF spike-phase histograms correspond to TPSM phase distributions of spikes discharged by a given place cell (or episode cell in the wheel) within its place field (or episode field in the wheel).

IN-PF signal phase histograms (Φ [LFP]; Figure 7A) represent the distribution of instantaneous (LFP: 1.25 kHz) TPSM phases for each time stamp the animal spent within a given place field.

Phase modulation of firing activity or signal (LFP) was tested for each individual cell by using the Rayleigh test (nonuniformity of the circular distribution). When phase modulation was significant ($p < 0.05$), Von Mises parameters μ and κ were estimated via maximum likelihood as indices of preferred phase and modulation strength, respectively. Statistical comparisons between phase distributions were performed by using the Kuiper test, a circular analog to the Kolmogorov-Smirnov test. Analyses were partly performed with a circular statistics Matlab toolbox (Berens, 2009).

In the maze and wheel, TPSM-phase maps (Figure 7B) and mean TPSM-phase values (Figures 7C and 7D, 8A, and S4) were obtained by binning the environment (either [1] relative to space, as square pixels of 2 × 2 cm [Figure 7B] or as normalized position in the run [Figure 7C], or [2] relative to elapsed time in the run [Figures 7D, 8A, and S4]) and computing the mean TPSM-phase distribution of the LFP signal in each bin (one value per space bin per animal run). The statistical significance of these results was further confirmed using a shuffling procedure consisting in a run per run random shift of TPSM phase (Figure S3).

Spatial Information Content

The spatial information content was quantified by using the Skaggs field specificity index (Markus et al., 1994), in which the information (in bits per spike) carried by the action potentials of a given cell is calculated by the formula $I = \Sigma Pi(\lambda i/\lambda)\log2(\lambda i/\lambda)$, where λi is the mean firing rate in bin i, λ is the overall mean firing rate, and Pi is the occupancy probability of bin i. As a more general, extended use of Skaggs' "field specificity index" originally used to quantify the discrimination between the various bins of the environment (i.e., the relationship between occupancy probabilities and firing rates in the various bins of a systematically partitioned space), we have considered various spatial partitioning of the environment and calculated the related spatial information content by using the same formula considering only two bins (IN versus OUT of a cell's place-field; within one versus the other place field of a multi-place-field cell). We have also considered partitioning between nonspatial criteria such as IN versus OUT of a cell's episode-field in the wheel (which is related to time rather than to space) or future maze-arm-running direction (next-left versus next-right runs in the wheel) and calculated the corresponding "discrimination" information content relating the events probabilities and their

associated relative firing rates. Therefore, in our analysis of inside (IN-PF) versus outside (OUT-PF) place field discrimination, spatial information content is related to the probability that the animal is either inside or outside the cell's place field when this given cell is firing an action potential. The same applies for the discrimination between two distinct episode fields in the wheel, between two distinct place fields/episode fields, or between next-left versus next-right runs in the wheel.

The net gain of information from taking TPSM phase into account was calculated for each cell by difference between the mean information content carried by the 20% of the total number of spikes discharged by the cell near its place field (or episode field or next-left/next-right runs in the wheel) preferred TPSM-phase (phase IN) and the average information content of the same number of spikes taken at systematically shifted TPSM-phases (all phases: 20 spike subsets, each discharged around a distinct TPSM phase determined as an incremental $\pi/10$ systematic phase offset relative to the preferred phase). Therefore, we have quantified how much information (in bits per spike) was added to the spikes discharged by an individual cell by taking into account the TPSM phase at which each of these spikes were fired.

The paired Student's t test was used for statistical comparisons (complete numerical values for the statistic are provided as Table S2). Unless stated otherwise, values are presented as mean ± SEM.

SUPPLEMENTAL INFORMATION

Supplemental Information includes seven figures, two tables, and Supplemental Experimental Procedures and can be found with this article online at http://dx.doi.org/10.1016/j.neuron.2012.06.036.

ACKNOWLEDGMENTS

This work was performed thanks to the following funding sources: INSERM (X.L.), FRM (X.L.), CNRS (X.L., J.O.), Région Aquitaine (X.L.), ENI-Net (X.L.), ANR (X.L. and C.M.). We wish to thank E. Pastalkova and G. Buzsáki for maze and wheel data, J. Csicsvari, K.D. Harris, L. Hazan and M. Zugaro for analysis software, Partha Mitra for advices regarding theta power analysis tools, John Finlayson for editing the manuscript, Thomas Leinekugel for Matlab programming, John Finlayson for thoroughly editing the manuscript, Anna Beyeler, Michele Pignatelli, Yannick Jeantet, and Thibault Maviel for useful comments and discussion. C.M. and X.L. designed the study, performed analysis, and wrote the manuscript; X.L. and H.H. performed experimental recordings, J.O. participated in clustering, Y.Y. provided support in analysis and funding of the project.

Accepted: June 26, 2012
Published: September 5, 2012

REFERENCES

Berens, P. (2009). CircStat: A MATLAB Toolbox for Circular Statistics. J. Stat. Softw. *31*, 1–21.

Bland, B.H., and Oddie, S.D. (2001). Theta band oscillation and synchrony in the hippocampal formation and associated structures: the case for its role in sensorimotor integration. Behav. Brain Res. *127*, 119–136.

Bragin, A., Jandó, G., Nádasdy, Z., Hetke, J., Wise, K., and Buzsáki, G. (1995). Gamma (40-100 Hz) oscillation in the hippocampus of the behaving rat. J. Neurosci. *15*, 47–60.

Bruns, A. (2004). Fourier-, Hilbert- and wavelet-based signal analysis: are they really different approaches? J. Neurosci. Methods *137*, 321–332.

Canolty, R.T., Edwards, E., Dalal, S.S., Soltani, M., Nagarajan, S.S., Kirsch, H.E., Berger, M.S., Barbaro, N.M., and Knight, R.T. (2006). High gamma power is phase-locked to theta oscillations in human neocortex. Science *313*, 1626–1628.

Chrobak, J.J., and Buzsáki, G. (1998). Gamma oscillations in the entorhinal cortex of the freely behaving rat. J. Neurosci. *18*, 388–398.

Czurkó, A., Hirase, H., Csicsvari, J., and Buzsáki, G. (1999). Sustained activation of hippocampal pyramidal cells by 'space clamping' in a running wheel. Eur. J. Neurosci. *11*, 344–352.

DeCoteau, W.E., Thorn, C., Gibson, D.J., Courtemanche, R., Mitra, P., Kubota, Y., and Graybiel, A.M. (2007). Learning-related coordination of striatal and hippocampal theta rhythms during acquisition of a procedural maze task. Proc. Natl. Acad. Sci. USA *104*, 5644–5649.

Dragoi, G., and Tonegawa, S. (2011). Preplay of future place cell sequences by hippocampal cellular assemblies. Nature *469*, 397–401.

Dragoi, G., Harris, K.D., and Buzsáki, G. (2003). Place representation within hippocampal networks is modified by long-term potentiation. Neuron *39*, 843–853.

Drew, P.J., Duyn, J.H., Golanov, E., and Kleinfeld, D. (2008). Finding coherence in spontaneous oscillations. Nat. Neurosci. *11*, 991–993.

Hinman, J.R., Penley, S.C., Long, L.L., Escabí, M.A., and Chrobak, J.J. (2011). Septotemporal variation in dynamics of theta: speed and habituation. J. Neurophysiol. *105*, 2675–2686.

Huxter, J., Burgess, N., and O'Keefe, J. (2003). Independent rate and temporal coding in hippocampal pyramidal cells. Nature *425*, 828–832.

Huxter, J.R., Senior, T.J., Allen, K., and Csicsvari, J. (2008). Theta phase-specific codes for two-dimensional position, trajectory and heading in the hippocampus. Nat. Neurosci. *11*, 587–594.

Jensen, O., and Lisman, J.E. (2000). Position reconstruction from an ensemble of hippocampal place cells: contribution of theta phase coding. J. Neurophysiol. *83*, 2602–2609.

Karashima, A., Nakao, M., Katayama, N., and Honda, K. (2005). Instantaneous acceleration and amplification of hippocampal theta wave coincident with phasic pontine activities during REM sleep. Brain Res. *1051*, 50–56.

Khanna, S.M., and Teich, M.C. (1989). Spectral characteristics of the responses of primary auditory-nerve fibers to amplitude-modulated signals. Hear. Res. *39*, 143–157.

Kramis, R., Vanderwolf, C.H., and Bland, B.H. (1975). Two types of hippocampal rhythmical slow activity in both the rabbit and the rat: relations to behavior and effects of atropine, diethyl ether, urethane, and pentobarbital. Exp. Neurol. *49*, 58–85.

Lakatos, P., Shah, A.S., Knuth, K.H., Ulbert, I., Karmos, G., and Schroeder, C.E. (2005). An oscillatory hierarchy controlling neuronal excitability and stimulus processing in the auditory cortex. J. Neurophysiol. *94*, 1904–1911.

Lakatos, P., Karmos, G., Mehta, A.D., Ulbert, I., and Schroeder, C.E. (2008). Entrainment of neuronal oscillations as a mechanism of attentional selection. Science *320*, 110–113.

Lee, M.G., Chrobak, J.J., Sik, A., Wiley, R.G., and Buzsáki, G. (1994). Hippocampal theta activity following selective lesion of the septal cholinergic system. Neuroscience *62*, 1033–1047.

Leopold, D.A., Murayama, Y., and Logothetis, N.K. (2003). Very slow activity fluctuations in monkey visual cortex: implications for functional brain imaging. Cereb. Cortex *13*, 422–433.

Leung, L.S. (1984a). Pharmacology of theta phase shift in the hippocampal CA1 region of freely moving rats. Electroencephalogr. Clin. Neurophysiol. *58*, 457–466.

Leung, L.S. (1984b). Theta rhythm during REM sleep and waking: correlations between power, phase and frequency. Electroencephalogr. Clin. Neurophysiol. *58*, 553–564.

Leutgeb, J.K., Leutgeb, S., Moser, M.B., and Moser, E.I. (2007). Pattern separation in the dentate gyrus and CA3 of the hippocampus. Science *315*, 961–966.

Louie, K., and Wilson, M.A. (2001). Temporally structured replay of awake hippocampal ensemble activity during rapid eye movement sleep. Neuron *29*, 145–156.

Markus, E.J., Barnes, C.A., McNaughton, B.L., Gladden, V.L., and Skaggs, W.E. (1994). Spatial information content and reliability of hippocampal CA1 neurons: effects of visual input. Hippocampus *4*, 410–421.

Maurer, A.P., Cowen, S.L., Burke, S.N., Barnes, C.A., and McNaughton, B.L. (2006). Organization of hippocampal cell assemblies based on theta phase precession. Hippocampus *16*, 785–794.

McFarland, W.L., Teitelbaum, H., and Hedges, E.K. (1975). Relationship between hippocampal theta activity and running speed in the rat. J. Comp. Physiol. Psychol. *88*, 324–328.

Mitra, P.P., and Bokil, H. (2008). Observed Brain Dynamics (New York: Oxford University Press).

Montgomery, S.M., Sirota, A., and Buzsáki, G. (2008). Theta and gamma coordination of hippocampal networks during waking and rapid eye movement sleep. J. Neurosci. *28*, 6731–6741.

Montgomery, S.M., Betancur, M.I., and Buzsáki, G. (2009). Behavior-dependent coordination of multiple theta dipoles in the hippocampus. J. Neurosci. *29*, 1381–1394.

Nir, Y., Mukamel, R., Dinstein, I., Privman, E., Harel, M., Fisch, L., Gelbard-Sagiv, H., Kipervasser, S., Andelman, F., Neufeld, M.Y., et al. (2008). Interhemispheric correlations of slow spontaneous neuronal fluctuations revealed in human sensory cortex. Nat. Neurosci. *11*, 1100–1108.

O'Keefe, J., and Dostrovsky, J. (1971). The hippocampus as a spatial map. Preliminary evidence from unit activity in the freely-moving rat. Brain Res. *34*, 171–175.

O'Keefe, J., and Recce, M.L. (1993). Phase relationship between hippocampal place units and the EEG theta rhythm. Hippocampus *3*, 317–330.

Pastalkova, E., Itskov, V., Amarasingham, A., and Buzsáki, G. (2008). Internally generated cell assembly sequences in the rat hippocampus. Science *321*, 1322–1327.

Rivas, J., Gaztelu, J.M., and García-Austt, E. (1996). Changes in hippocampal cell discharge patterns and theta rhythm spectral properties as a function of walking velocity in the guinea pig. Exp. Brain Res. *108*, 113–118.

Robinson, T.E., Kramis, R.C., and Vanderwolf, C.H. (1977). Two types of cerebral activation during active sleep: relations to behavior. Brain Res. *124*, 544–549.

Sainsbury, R.S., Harris, J.L., and Rowland, G.L. (1987a). Sensitization and hippocampal type 2 theta in the rat. Physiol. Behav. *41*, 489–493.

Sainsbury, R.S., Heynen, A., and Montoya, C.P. (1987b). Behavioral correlates of hippocampal type 2 theta in the rat. Physiol. Behav. *39*, 513–519.

Sano, K., Iwahara, S., Senba, K., Sano, A., and Yamazaki, S. (1973). Eye movements and hippocampal theta activity in rats. Electroencephalogr. Clin. Neurophysiol. *35*, 621–625.

Shen, J., Barnes, C.A., McNaughton, B.L., Skaggs, W.E., and Weaver, K.L. (1997). The effect of aging on experience-dependent plasticity of hippocampal place cells. J. Neurosci. *17*, 6769–6782.

Skaggs, W.E., McNaughton, B.L., Wilson, M.A., and Barnes, C.A. (1996). Theta phase precession in hippocampal neuronal populations and the compression of temporal sequences. Hippocampus *6*, 149–172.

Sutherland, R.J., Whishaw, I.Q., and Regehr, J.C. (1982). Cholinergic receptor blockade impairs spatial localization by use of distal cues in the rat. J. Comp. Physiol. Psychol. *96*, 563–573.

Vanderwolf, C.H. (1969). Hippocampal electrical activity and voluntary movement in the rat. Electroencephalogr. Clin. Neurophysiol. *26*, 407–418.

Whishaw, I.Q. (1972). Hippocampal electroencephalographic activity in the Mongolian gerbil during natural behaviours and wheel running and in the rat during wheel running and conditioned immobility. Can. J. Psychol. *26*, 219–239.

Whishaw, I.Q., and Dyck, R. (1984). Comparative potency of tactile, auditory, and visual stimulus repetition in eliciting activated forebrain EEG in the rabbit. Behav. Neurosci. *98*, 333–344.

Whishaw, I.Q., and Vanderwolf, C.H. (1973). Hippocampal EEG and behavior: changes in amplitude and frequency of RSA (theta rhythm) associated with spontaneous and learned movement patterns in rats and cats. Behav. Biol. *8*, 461–484.